Chapter 2

The Coriolis Force

ABSTRACT
The objective of this chapter is to examine the Coriolis force, a fictitious force arising from the choice of a rotating framework of reference. Some physical considerations are offered to provide insight on this nonintuitive but essential element of geophysical flows. The numerical section of this chapter treats time stepping introduced in the particular case of inertial oscillations and generalized afterwards.

2.1 ROTATING FRAMEWORK OF REFERENCE

From a theoretical point of view, all equations governing geophysical fluid processes could be stated with respect to an inertial framework of reference, fixed with respect to distant stars. But, we people on Earth observe fluid motions with respect to this rotating system. Also, mountains and ocean boundaries are stationary with respect to Earth. Common sense therefore dictates that we write the governing equations in a reference framework rotating with our planet. (The same can be said for other planets and stars.) The trouble arising from the additional terms in the equations of motion is less than that which would arise from having to reckon with moving boundaries and the need to subtract systematically the ambient rotation from the resulting flow.

To facilitate the mathematical developments, let us first investigate the two-dimensional case (Fig. 2.1). Let the X– and Y–axes form the inertial framework of reference and the x– and y–axes be those of a framework with the same origin but rotating at the angular rate Ω (defined as positive in the trigonometric sense). The corresponding unit vectors are denoted ($\mathbf{I}$, $\mathbf{J}$) and ($\mathbf{i}$, $\mathbf{j}$). At any time t, the rotating x–axis makes an angle Ωt with the fixed X–axis. It follows that

$$\mathbf{i} = +\mathbf{I}\cos\Omega t + \mathbf{J}\sin\Omega t \quad (2.1a) \qquad \mathbf{I} = +\mathbf{i}\cos\Omega t - \mathbf{j}\sin\Omega t \quad (2.2a)$$

$$\mathbf{j} = -\mathbf{I}\sin\Omega t + \mathbf{J}\cos\Omega t \quad (2.1b) \qquad \mathbf{J} = +\mathbf{i}\sin\Omega t + \mathbf{j}\cos\Omega t, \quad (2.2b)$$

Introduction to Geophysical Fluid Dynamics, Volume 101, ISSN 0074-6142, DOI: 10.1016/B978-0-12-088759-0.00002-X

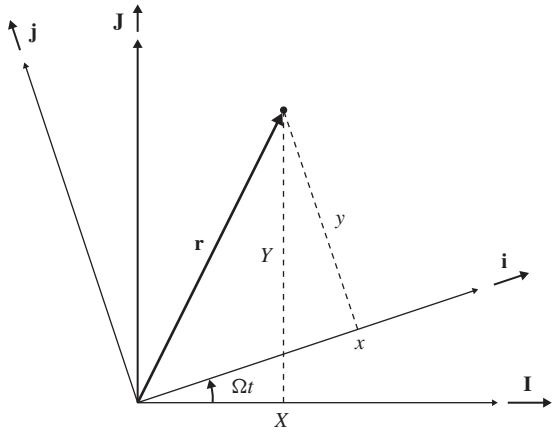

FIGURE 2.1 Fixed (X, Y) and rotating (x, y) frameworks of reference.

and that the coordinates of the position vector $\mathbf{r} = X\mathbf{I} + Y\mathbf{J} = x\mathbf{i} + y\mathbf{j}$ of any point in the plane are related by

$$x = +X\cos\Omega t + Y\sin\Omega t \tag{2.3a}$$

$$y = -X\sin\Omega t + Y\cos\Omega t. \tag{2.3b}$$

The first time derivative of the preceding expressions yields

$$\frac{\mathrm{d}x}{\mathrm{d}t} = +\frac{\mathrm{d}X}{\mathrm{d}t}\cos\Omega t + \frac{\mathrm{d}Y}{\mathrm{d}t}\sin\Omega t \overbrace{-\Omega X\sin\Omega t + \Omega Y\cos\Omega t}^{+\Omega y} \tag{2.4a}$$

$$\frac{\mathrm{d}y}{\mathrm{d}t} = -\frac{\mathrm{d}X}{\mathrm{d}t}\sin\Omega t + \frac{\mathrm{d}Y}{\mathrm{d}t}\cos\Omega t \underbrace{-\Omega X\cos\Omega t - \Omega Y\sin\Omega t}_{-\Omega x}. \tag{2.4b}$$

The quantities $\mathrm{d}x/\mathrm{d}t$ and $\mathrm{d}y/\mathrm{d}t$ give the rates of change of the coordinates relative to the moving frame as time evolves. They are thus the components of the relative velocity:

$$\mathbf{u} = \frac{\mathrm{d}x}{\mathrm{d}t}\mathbf{i} + \frac{\mathrm{d}y}{\mathrm{d}t}\mathbf{j} = u\mathbf{i} + v\mathbf{j}. \tag{2.5}$$

Similarly, $\mathrm{d}X/\mathrm{d}t$ and $\mathrm{d}Y/\mathrm{d}t$ give the rates of change of the absolute coordinates and form the absolute velocity:

$$\mathbf{U} = \frac{\mathrm{d}X}{\mathrm{d}t}\mathbf{I} + \frac{\mathrm{d}Y}{\mathrm{d}t}\mathbf{J}.$$

Writing the absolute velocity in terms of the rotating unit vectors, we obtain [using Eq. (2.2)]

$$\begin{aligned}\mathbf{U} &= \left(\frac{\mathrm{d}X}{\mathrm{d}t}\cos\Omega t + \frac{\mathrm{d}Y}{\mathrm{d}t}\sin\Omega t\right)\mathbf{i} + \left(-\frac{\mathrm{d}X}{\mathrm{d}t}\sin\Omega t + \frac{\mathrm{d}Y}{\mathrm{d}t}\cos\Omega t\right)\mathbf{j} \\ &= U\mathbf{i} + V\mathbf{j}. \end{aligned} \tag{2.6}$$

Thus, $\mathrm{d}X/\mathrm{d}t$ and $\mathrm{d}Y/\mathrm{d}t$ are the components of the absolute velocity $\mathbf{U}$ in the inertial frame, whereas U and V are the components of the same vector in the rotating frame. Use of Eqs. (2.4) and (2.3) in the preceding expression yields the following relations between absolute and relative velocities:

$$U = u - \Omega y, \quad V = v + \Omega x. \tag{2.7}$$

These equalities simply state that the absolute velocity is the relative velocity plus the entraining velocity due to the rotation of the reference framework.

A second derivative with respect to time provides in a similar manner:

$$\begin{aligned}\frac{\mathrm{d}^2x}{\mathrm{d}t^2} &= \left(\frac{\mathrm{d}^2X}{\mathrm{d}t^2}\cos\Omega t + \frac{\mathrm{d}^2Y}{\mathrm{d}t^2}\sin\Omega t\right) + 2\Omega\underbrace{\left(-\frac{\mathrm{d}X}{\mathrm{d}t}\sin\Omega t + \frac{\mathrm{d}Y}{\mathrm{d}t}\cos\Omega t\right)}_{V} \\ &\quad - \Omega^2\underbrace{(X\cos\Omega t + Y\sin\Omega t)}_{x} \end{aligned} \tag{2.8a}$$

$$\begin{aligned}\frac{\mathrm{d}^2y}{\mathrm{d}t^2} &= \left(-\frac{\mathrm{d}^2X}{\mathrm{d}t^2}\sin\Omega t + \frac{\mathrm{d}^2Y}{\mathrm{d}t^2}\cos\Omega t\right) - 2\Omega\underbrace{\left(\frac{\mathrm{d}X}{\mathrm{d}t}\cos\Omega t + \frac{\mathrm{d}Y}{\mathrm{d}t}\sin\Omega t\right)}_{U} \\ &\quad - \Omega^2\underbrace{(-X\sin\Omega t + Y\cos\Omega t)}_{y}. \end{aligned} \tag{2.8b}$$

Expressed in terms of the relative and absolute accelerations

$$\begin{aligned}\mathbf{a} &= \frac{\mathrm{d}^2x}{\mathrm{d}t^2}\mathbf{i} + \frac{\mathrm{d}^2y}{\mathrm{d}t^2}\mathbf{j} = \frac{\mathrm{d}u}{\mathrm{d}t}\mathbf{i} + \frac{\mathrm{d}v}{\mathrm{d}t}\mathbf{j} = a\mathbf{i} + b\mathbf{j} \\ \mathbf{A} &= \frac{\mathrm{d}^2X}{\mathrm{d}t^2}\mathbf{I} + \frac{\mathrm{d}^2Y}{\mathrm{d}t^2}\mathbf{J} \\ &= \left(\frac{\mathrm{d}^2X}{\mathrm{d}t^2}\cos\Omega t + \frac{\mathrm{d}^2Y}{\mathrm{d}t^2}\sin\Omega t\right)\mathbf{i} + \left(\frac{\mathrm{d}^2Y}{\mathrm{d}t^2}\cos\Omega t - \frac{\mathrm{d}^2X}{\mathrm{d}t^2}\sin\Omega t\right)\mathbf{j} = A\mathbf{i} + B\mathbf{j}, \end{aligned}$$

expressions (2.8) condense to

$$a = A + 2\Omega V - \Omega^2 x, \quad b = B - 2\Omega U - \Omega^2 y.$$

In analogy with the absolute velocity vector, d^2X/dt^2 and d^2Y/dt^2 are the components of the absolute acceleration **A** in the inertial frame, whereas A and B are the components of the same vector in the rotating frame. The absolute acceleration components, necessary later to formulate Newton's law, are obtained by solving for A and B and using Eq. (2.7):

$$A = a - 2\Omega v - \Omega^2 x, \quad B = b + 2\Omega u - \Omega^2 y. \tag{2.9}$$

We now see that the difference between absolute and relative acceleration consists of two contributions. The first, proportional to Ω and to the relative velocity, is called the Coriolis acceleration; the other, proportional to Ω^2 and to the coordinates, is called the centrifugal acceleration. When placed on the other side of the equality in Newton's law, these terms can be assimilated to forces (per unit mass). The centrifugal force acts as an outward pull, whereas the Coriolis force depends on the direction and magnitude of the relative velocity.

Formally, the preceding results could have been derived in a vector form. Defining the vector rotation

$$\boldsymbol{\Omega} = \Omega \mathbf{k},$$

where **k** is the unit vector in the third dimension (which is common to both systems of reference), we can write Eqs. (2.7) and (2.9) as

$$\begin{aligned} \mathbf{U} &= \mathbf{u} + \boldsymbol{\Omega} \times \mathbf{r} \\ \mathbf{A} &= \mathbf{a} + 2\boldsymbol{\Omega} \times \mathbf{u} + \boldsymbol{\Omega} \times (\boldsymbol{\Omega} \times \mathbf{r}), \end{aligned} \tag{2.10}$$

where the symbol $\times$ indicates the vectorial product. This implies that taking a time derivative of a vector with respect to the inertial framework is equivalent to applying the operator

$$\frac{d}{dt} + \boldsymbol{\Omega} \times$$

in the rotating framework of reference.

A very detailed exposition of the Coriolis and centrifugal accelerations can be found in the book by Stommel and Moore (1989). In addition, the reader will find a historical perspective in Ripa (1994) and laboratory illustrations in Marshall and Plumb (2008).

2.2 UNIMPORTANCE OF THE CENTRIFUGAL FORCE

Unlike the Coriolis force, which is proportional to the velocity, the centrifugal force depends solely on the rotation rate and the distance of the particle to the rotation axis. Even at rest with respect to the rotating planet, particles experience an outward pull. Yet, on the earth as on other planetary bodies, objects don't fly out to space. How is that possible? Obviously, gravity keeps everything together.

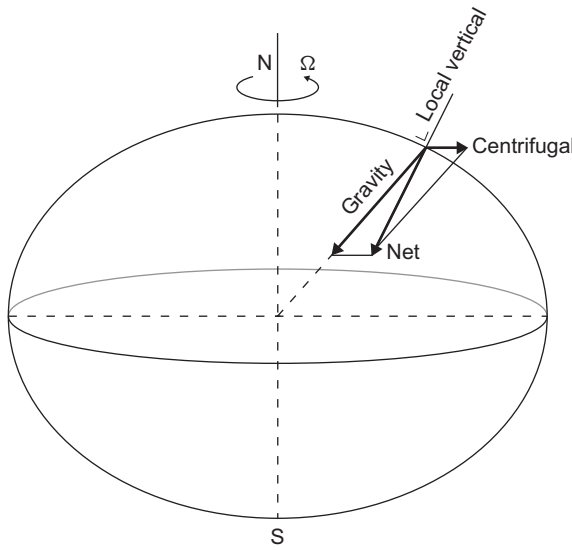

FIGURE 2.2 How the flattening of the rotating earth (grossly exaggerated in this drawing) causes the gravitational and centrifugal forces to combine into a net force aligned with the local vertical, so that equilibrium is reached.

In the absence of rotation, gravitational forces keep the matter together to form a spherical body (with the denser materials at the center and the lighter ones on the periphery). The outward pull caused by the centrifugal force distorts this spherical equilibrium, and the planet assumes a slightly flattened shape. The degree of flattening is precisely that necessary to keep the planet in equilibrium for its rotation rate.

The situation is depicted in Fig. 2.2. By its nature, the centrifugal force is directed outward, perpendicular to the axis of rotation, whereas the gravitational force points toward the planet's center. The resulting force assumes an intermediate direction, and this direction is precisely the direction of the local vertical. Indeed, under this condition, a loose particle would have no tendency of its own to fly away from the planet. In other words, every particle at rest on the surface will remain at rest unless it is subjected to additional forces.

The flattening of the earth, as well as that of other celestial bodies in rotation, is important to neutralize the centrifugal force. But, this is not to say that it greatly distorts the geometry. On the earth, for example, the distortion is very slight because gravity by far exceeds the centrifugal force; the terrestrial equatorial radius is 6378 km, slightly greater than its polar radius of 6357 km. The shape of the rotating oblate earth is treated in detail by Stommel and Moore (1989) and by Ripa (1994).

For the sake of simplicity in all that follows, we will call the gravitational force the resultant force, aligned with the vertical and equal to the sum of the

true gravitational force and the centrifugal force. Due to inhomogeneous distributions of rocks and magma on Earth, the true gravitational force is not directed toward the center of the earth. For the same reason as the centrifugal force has rendered the earth surface oblate, this inhomogeneous true gravity has deformed the earth surface until the total (apparent) gravitational force is perpendicular to it. The surface so obtained is called a *geoid* and can be interpreted as the surface of an ocean at rest (with a continuous extension on land). This virtual continuous surface is perpendicular at every point to the direction of gravity (including the centrifugal force) and forms an *equipotential* surface, meaning that a particle moving on that surface undergoes no change in potential energy. The value of this potential energy per unit mass is called the geopotential, and the geoid is thus a surface of constant geopotential. This surface will be the reference surface from which land elevations, (dynamic) sea surface elevations, and ocean depth will be defined. For more on the geoid, the reader is referred to Robinson (2004), Chapter 11.

In a rotating laboratory tank, the situation is similar but not identical. The rotation causes a displacement of the fluid toward the periphery. This proceeds until the resulting inward pressure gradient prevents any further displacement. Equilibrium then requires that at any point on the surface, the downward gravitational force and the outward centrifugal force combine into a resultant force normal to the surface (Fig. 2.3), so that the surface becomes an equipotential surface. Although the surface curvature is crucial in neutralizing the centrifugal force, the vertical displacements are rather small. In a tank rotating at the rate of one revolution every 2 s (30 rpm) and 40 cm in diameter, the difference in fluid height between the rim and the center is a modest 2 cm.

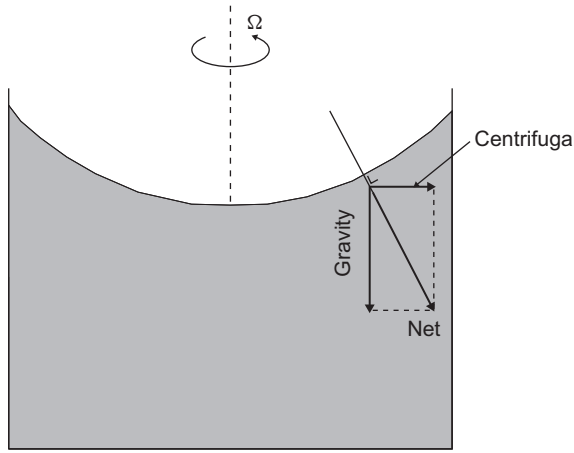

FIGURE 2.3 Equilibrium surface of a rotating fluid in an open container. The surface slope is such that gravitational and centrifugal forces combine into a net force everywhere aligned with the local normal to the surface.

2.3 FREE MOTION ON A ROTATING PLANE

The preceding argument allows us to combine the centrifugal force with the gravitational force, but the Coriolis force remains. To have an idea of what this force can cause, let us examine the motion of a free particle, that is, a particle not subject to any external force other than apparent gravity (true gravity combined with centrifugal force) on the horizontal plane extending from the North Pole.

If the particle is free of any force in this plane, its acceleration in the inertial frame is nil, by Newton's law. According to Eq. (2.9), with the centrifugal-acceleration terms no longer present, the equations governing the velocity components of the particle are

$$\frac{\mathrm{d}u}{\mathrm{d}t} - 2\Omega v = 0, \quad \frac{\mathrm{d}v}{\mathrm{d}t} + 2\Omega u = 0. \tag{2.11}$$

The general solution to this system of linear equations is

$$u = V\sin(ft+\phi), \quad v = V\cos(ft+\phi), \tag{2.12}$$

where $f = 2\Omega$, called the Coriolis parameter, has been introduced for convenience, and V and ϕ are two arbitrary constants of integration. Without loss of generality, V can always be chosen as nonnegative. (Do not confuse this constant V with the y–component of the absolute velocity introduced in Section 2.1.) A first result is that the particle speed $(u^2+v^2)^{1/2}$ remains unchanged in time. It is equal to V, a constant determined by the initial conditions.

Although the speed remains unchanged, the components u and v do depend on time, implying a change in direction. To document this curving effect, it is most instructive to derive the trajectory of the particle. The coordinates of the particle position change, by definition of the vector velocity, according to $\mathrm{d}x/\mathrm{d}t = u$ and $\mathrm{d}y/\mathrm{d}t = v$, and a second time integration provides

$$x = x_0 - \frac{V}{f}\cos(ft+\phi) \tag{2.13a}$$

$$y = y_0 + \frac{V}{f}\sin(ft+\phi), \tag{2.13b}$$

where x_0 and y_0 are additional constants of integration to be determined from the initial coordinates of the particle. From the last relations, it follows directly that

$$(x-x_0)^2 + (y-y_0)^2 = \left(\frac{V}{f}\right)^2. \tag{2.14}$$

This implies that the trajectory is a circle centered at (x_0, y_0) and of radius $V/|f|$. The situation is depicted in Fig. 2.4.

In the absence of rotation ($f = 0$), this radius is infinite, and the particle follows a straight path, as we could have anticipated. But, in the presence of

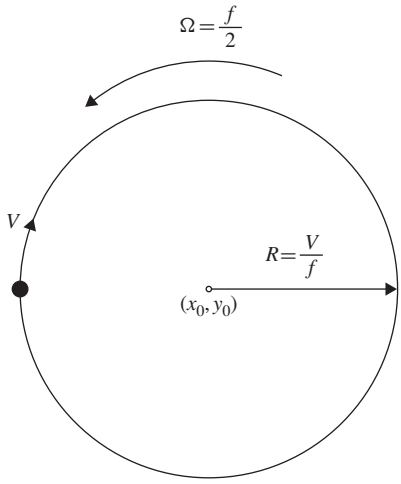

FIGURE 2.4 Inertial oscillation of a free particle on a rotating plane. The orbital period is exactly half of the ambient revolution period. This figure has been drawn with a positive Coriolis parameter, f, representative of the northern hemisphere. If f were negative (as in the southern hemisphere), the particle would veer to the left.

rotation ($f \neq 0$), the particle turns constantly. A quick examination of Eq. (2.13) reveals that the particle turns to the right (clockwise) if f is positive or to the left (counterclockwise) if $f$is negative. In sum, the rule is that the particle turns in the sense opposite to that of the ambient rotation.

At this point, we may wonder whether this particle rotation is none other than the negative of the ambient rotation, in such a way as to keep the particle at rest in the absolute frame of reference. But, there are at least two reasons why this is not so. The first is that the coordinates of the center of the particle's circular path are arbitrary and are therefore not required to coincide with those of the axis of rotation. The second and most compelling reason is that the two frequencies of rotation are simply not the same: the ambient rotating plane completes one revolution in a time equal to $T_a = 2\pi/\Omega$, whereas the particle covers a full circle in a time equal to $T_p = 2\pi/f = \pi/\Omega$, called *inertial period*. Thus, the particle goes around its orbit twice as the plane accomplishes a single revolution.

The spontaneous circling of a free particle endowed with an initial velocity in a rotating environment bears the name of *inertial oscillation*. Note that, since the particle speed can vary, so can the inertial radius, $V/|f|$, whereas the frequency, $|f| = 2|\Omega|$, is a property of the rotating environment and is independent of the initial conditions.

The preceding exercise may appear rather mathematical and devoid of any physical interpretation. There exists, however, a geometric argument and a physical analogy. Let us first discuss the geometric argument. Consider a rotating table and, on it, a particle initially ($t = 0$) at a distance R from the axis of rotation, approaching the latter at a speed u (Fig. 2.5). At some later time t, the particle has approached the axis of rotation by a distance ut while it has covered

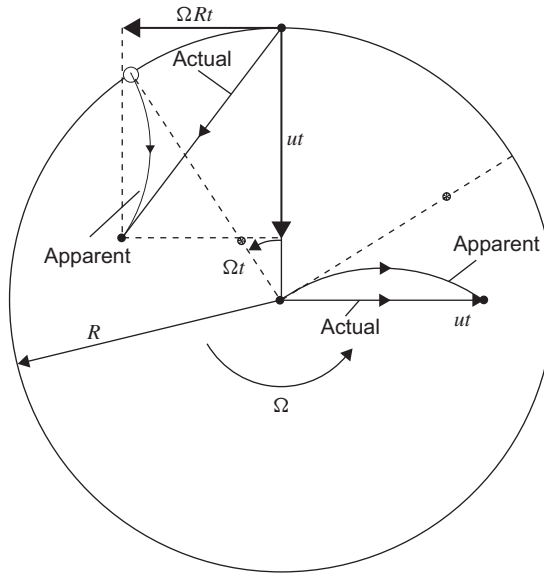

FIGURE 2.5 Geometrical interpretation of the apparent veering of a particle trajectory viewed in a rotating framework. The veering is to the right when the ambient rotation is counterclockwise, as shown here for two particular trajectories, one originating from the rim and the other from the axis of rotation.

the distance ΩRt laterally. It now lies at the position indicated by a solid dot. During the lapse t, the table has rotated by an angle Ωt, and to an observer rotating with the table, the particle seems to have originated from the point on the rim indicated by the open circle. The construction shows that, although the actual trajectory is perfectly straight, the apparent path as noted by the observer rotating with the table curves to the right. A similar conclusion holds for a particle radially pushed away from the center with a speed u. In absolute axes, the trajectory is a straight line covering a distance ut from the center. During the lapse t, the table has rotated and for an observer on the rotating platform, the particle, instead of arriving in the location of the asterisk, apparently veered to the right.

The problem with this argument is that to construct the absolute trajectory, we chose a straight path, that is, we implicitly considered the total absolute acceleration, which in the rotating framework includes the centrifugal acceleration. The latter, however, should not have been retained for consistency with the case of terrestrial rotation, but because it is a radial force, it does not account for the transverse displacement. Therefore, the apparent veering is, at least for a short interval of time, entirely due to the Coriolis effect.

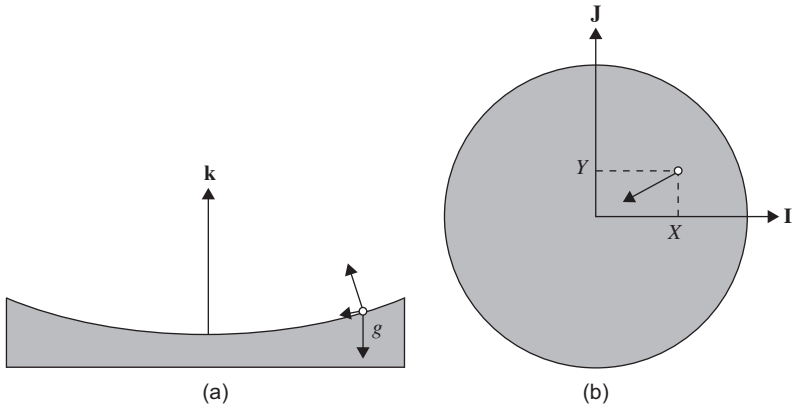

FIGURE 2.6 Side view (a) and top view (b) of a mass on a paraboloid surface.

2.4 ANALOGY AND PHYSICAL INTERPRETATION

Consider[1] a particle of a certain mass in a gravitational field g on a paraboloid surface (Fig. 2.6) of elevation Z given by

$$Z = \frac{\Omega^2}{2g}\left(X^2 + Y^2\right). \tag{2.15}$$

Provided that the paraboloid is sufficiently flat compared to its radius R ($\Omega^2 R/2g \ll 1$), the equations of motions of the mass are easily derived

$$\frac{\mathrm{d}^2X}{\mathrm{d}t^2} = -g\frac{\partial Z}{\partial X} = -\Omega^2 X, \quad \frac{\mathrm{d}^2Y}{\mathrm{d}t^2} = -g\frac{\partial Z}{\partial Y} = -\Omega^2 Y, \tag{2.16}$$

and describe a pendulum motion.

The frequency Ω measures the curvature of the surface and is the pendulum's natural frequency of oscillation. Note how the gravitational restoring force takes on the form of a negative centrifugal force. Without loss of generality, we can choose the initial position of the particle as $X = X_0$, $Y = 0$. In that location, we launch the particle with an initial velocity of $\mathrm{d}X/\mathrm{d}t = U_0$ and $\mathrm{d}Y/\mathrm{d}t = V_0$ in absolute axes. The trajectory in absolute axes is easily found as the solution of Eq. (2.16)

$$X = X_0 \cos\Omega t + \frac{U_0}{\Omega}\sin\Omega t \tag{2.17a}$$

$$Y = \frac{V_0}{\Omega}\sin\Omega t. \tag{2.17b}$$

[1] A similar analogy was suggested to the authors by Prof. Satoshi Sakai at Kyoto University.

Two particular solutions are noteworthy. If the initial condition is a pure radial displacement ($V_0 = 0$), the particle forever oscillates along the line $Y = 0$. The oscillation, of period $2\pi/\Omega$, takes it to the center twice per period, that is, every π/Ω time interval. At the other extreme, the particle can be imparted an initial azimuthal velocity of magnitude such that the outward centrifugal force of the ensuing circling motion exactly cancels the inward gravitational pull at that radial distance:

$$U_0 = 0, \quad V_0 = \pm\Omega X_0, \tag{2.18}$$

in which case the particle remains at a fixed distance from the center ($X^2 + Y^2 = X_0^2$) and circles at a constant angular rate Ω, counterclockwise or clockwise, depending on the direction of the initial azimuthal velocity.

Outside of these two extreme behaviors, the particle describes an elliptical trajectory of size, eccentricity, and phase related to the initial condition. The orbit does not take it through the center but brings it, twice per period, to a distance of closest approach (*perigee*) and, twice per period, to a distance of largest excursion (*apogee*).

At this point, the reader may rightfully wonder: Where is the analogy with the motion of a particle subject to the Coriolis force? To show this analogy, let us now view the particle motion in a rotating frame, but, of course, not any rotating frame: Let us select the angular rotation rate Ω equal to the particle's frequency of oscillation. This choice is made so that, in the rotating frame of reference, the outward centrifugal force is everywhere and at all times exactly canceled by the inward gravitational pull experienced on the parabolic surface. Thus, the equations of motion expressed in the rotating frame include only the relative acceleration and the Coriolis force, that is, they are none other than Eqs. (2.11).

Let us now consider the oscillations as seen by an observer in the rotating frame (Figs. 2.7 and 2.8). When the particle oscillates strictly back and forth, the rotating observer sees a curved trajectory. Because the particle passes by the origin twice per oscillation, the orbit seen by the rotating observer also passes by the origin twice per period. When the particle reaches its extreme displacement on one side, it reaches an apogee on its orbit as viewed in the rotating frame; then, by the time it reaches its maximum displacement on the opposite side, π/Ω later, the rotating framework has rotated exactly by half a turn, so that this second apogee of the orbit coincides with the first. Therefore, the reader can readily be convinced that the orbit in the rotating frame is drawn twice per period of oscillation. Algebraic or geometric developments reveal that the orbit in the rotating framework is circular (Fig. 2.8a).

In the other extreme situation, when the particle circles at a constant distance from the origin, two cases must be distinguished, depending on whether it circles in the direction of or opposite to the observer's rotating frame. If the direction is the same [positive sign in Eq. (2.18)], the observer simply chases the particle, which then appears stationary, and the orbit reduces to a single point (Fig. 2.8b). This case corresponds to the state of rest of a particle

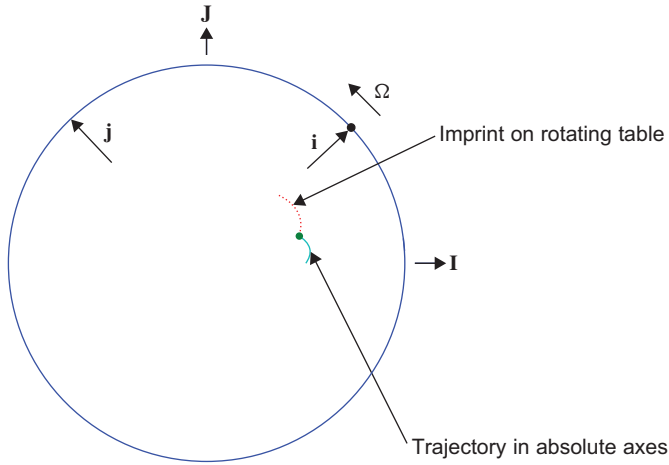

FIGURE 2.7 Oscillation of the paraboloid pendulum viewed in absolute axes. Dots represent the imprint of the mass on the paraboloid that rotates with the rotation rate Ω.

in a rotating environment [$V = 0$ in Eq. (2.12) through Eq. (2.13)]. If the sense of rotation is opposite [minus sign in Eq. (2.18)], the reference frame rotates at the rate Ω in one direction, whereas the particle circles at the same rate in the opposite direction. To the observer, the particle appears to rotate at the rate 2Ω. The orbit is obviously a circle centered at the origin and of radius equal to the particle's radial displacement; it is covered twice per revolution of the rotating frame (Fig. 2.8c). Finally, for arbitrary oscillations, the orbit in the rotating frame is a circle of finite radius that is not centered at the origin, does not pass by the origin, and may or may not include the origin (Fig. 2.8d). The reader may experiment with MATLAB™ code `parabolic.m` for further explorations of trajectories.

Looking at the system from an inertial framework, we observe that the oscillation of the particle is due to the restoring force of gravity. In particular, its projection on the parabolic surface is responsible for the tendency to move toward the center of the paraboloid. If we look from the rotating framework, this component of gravity is always cancelled by the centrifugal force associated with the rotation, and the restoring force responsible for the oscillation is now the Coriolis force.

2.5 ACCELERATION ON A THREE-DIMENSIONAL ROTATING PLANET

For all practical purposes, except as outlined earlier when the centrifugal force was discussed (Section 2.2), the earth can be taken as a perfect sphere. This sphere rotates about its North Pole–South Pole axis. At any given latitude φ,

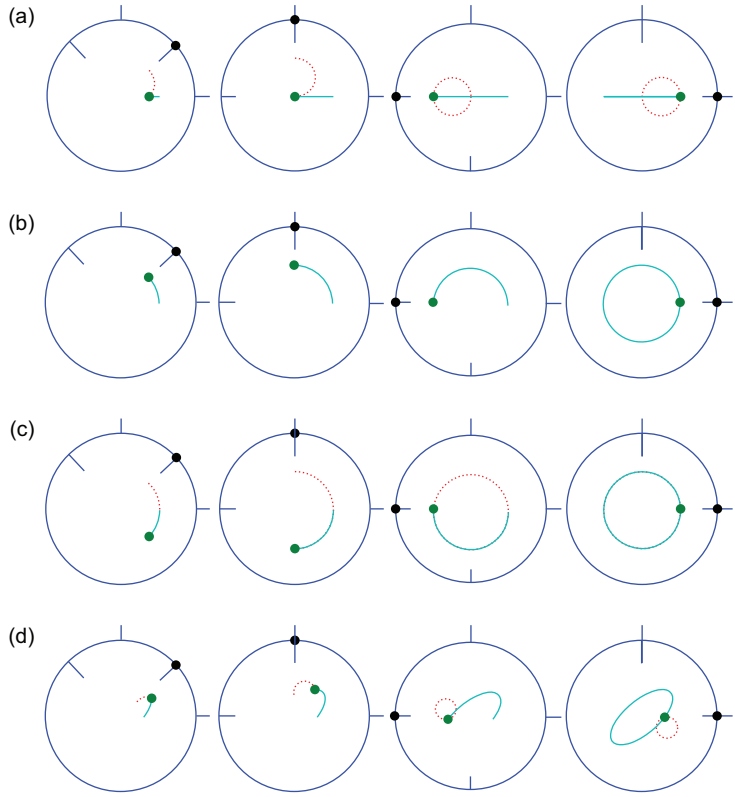

FIGURE 2.8 Orbits (full line) in absolute axes with imprint of trajectories (dots) on rotating framework (apparent trajectory). Each row shows the situation for a different initial condition and after 1/8, 1/4, 1/2, and a full period $2\pi\Omega^{-1}$. Orbits differ according to the initial velocity: the first row (a) shows oscillations obtained without initial velocity, the second row (b) was created with initial velocity $U_0 = 0,\ V_0 = X_0\Omega$, the third row (c) corresponds to the opposite initial velocity $U_0 = 0,\ V_0 = -X_0\Omega$, and the last row (d) corresponds to an arbitrary initial velocity.

the north–south direction departs from the local vertical, and the Coriolis force assumes a form different from that established in the preceding section.

Figure 2.9 depicts the traditional choice for a local Cartesian framework of reference: the x-axis is oriented eastward, the y-axis, northward, and the z-axis, upward. In this framework, the earth's rotation vector is expressed as

$$\boldsymbol{\Omega} = \Omega\cos\varphi\,\mathbf{j} + \Omega\sin\varphi\,\mathbf{k}. \tag{2.19}$$

The absolute acceleration minus the centrifugal component,

$$\frac{\mathrm{d}\mathbf{u}}{\mathrm{d}t} + 2\boldsymbol{\Omega}\times\mathbf{u},$$

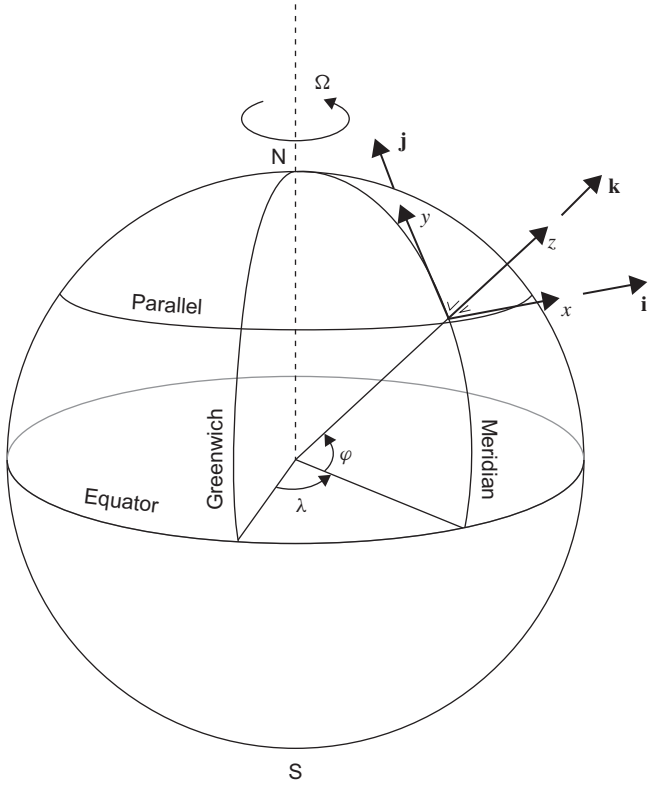

FIGURE 2.9 Definition of a local Cartesian framework of reference on a spherical Earth. The coordinate x is directed eastward, y northward, and z upward.

has the following three components:

$$x: \quad \frac{\mathrm{d}u}{\mathrm{d}t} + 2\Omega\cos\varphi\, w - 2\Omega\, \sin\varphi\, v \tag{2.20a}$$

$$y: \quad \frac{\mathrm{d}v}{\mathrm{d}t} + 2\Omega\sin\varphi\, u \tag{2.20b}$$

$$z: \quad \frac{\mathrm{d}w}{\mathrm{d}t} - 2\Omega\cos\varphi\, u. \tag{2.20c}$$

With x, y, and z everywhere aligned with the local eastward, northward, and vertical directions, the coordinate system is curvilinear, and additional terms arise in the components of the relative acceleration. These terms will be dismissed in Section 3.2 because of their relatively small size in most instances.

For convenience, we define the quantities

$$f = 2\Omega \sin\varphi \tag{2.21}$$

$$f_* = 2\Omega \cos\varphi. \tag{2.22}$$

The coefficient f is called the *Coriolis parameter*, whereas f_* has no traditional name and will be called here the *reciprocal Coriolis parameter*. In the northern hemisphere, f is positive; it is zero at the equator and negative in the southern hemisphere. In contrast, f_* is positive in both hemispheres and vanishes at the poles. An examination of the relative importance of the various terms (Section 4.3) will reveal that, generally, the f terms are important, whereas the f_* terms may be neglected.

Horizontal, unforced motions are described by

$$\frac{\mathrm{d}u}{\mathrm{d}t} - fv = 0 \tag{2.23a}$$

$$\frac{\mathrm{d}v}{\mathrm{d}t} + fu = 0 \tag{2.23b}$$

and are still characterized by solution (2.12). The difference resides in the value of f, now given by Eq. (2.21). Thus, inertial oscillations on Earth have periodicities equal to $2\pi/f = \pi/\Omega\sin\varphi$, ranging from 11 h 58' at the poles to infinity along the equator. Pure inertial oscillations are, however, quite rare because of the usual presence of pressure gradients and other forces. Nonetheless, inertial oscillations are not uncommonly found to contribute to observations of oceanic currents. An example of such an occurrence, where the inertial oscillations made up almost the entire signal, was reported by Gustafson and Kullenberg (1936). Current measurements in the Baltic Sea showed periodic oscillations about a mean value. When added to one another to form a so-called progressive vector diagram (Fig. 2.10), the currents distinctly showed a mean drift, on which were superimposed quite regular clockwise oscillations. The theory of inertial oscillation predicts clockwise rotation in the northern hemisphere with period of $2\pi/f = \pi/\Omega\sin\varphi$, or 14 h at the latitude of observations, thus confirming the interpretation of the observations as inertial oscillations.

2.6 NUMERICAL APPROACH TO OSCILLATORY MOTIONS

The equations of free motion on a rotating plane (2.11) have been considered in some detail in Section 2.3, and it is now appropriate to consider their discretization, as the corresponding terms are part of all numerical models of geophysical flows. Upon introducing the time increment Δt, an approximation to the components of the velocity will be determined at the discrete instants $t^n = n\Delta t$ with $n = 1, 2, 3, \ldots$, which are denoted $\tilde{u}^n = \tilde{u}(t_n)$ and $\tilde{v}^n = \tilde{v}(t_n)$, with tildes used to distinguish the discrete solution from the exact one. The so-called *Euler method*

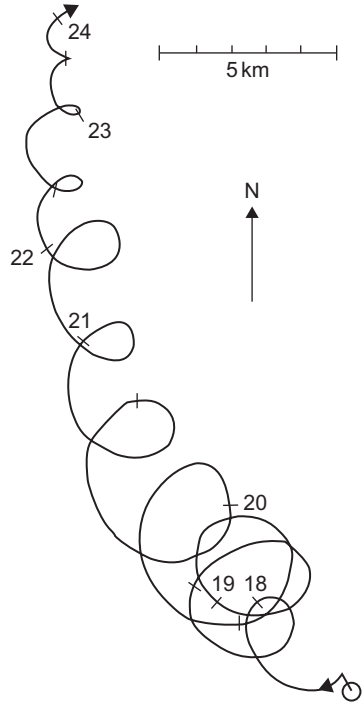

FIGURE 2.10 Evidence of inertial oscillations in the Baltic Sea, as reported by Gustafson and Kullenberg (1936). The plot is a progressive vector diagram constructed by the successive addition of velocity measurements at a fixed location. For weak or uniform velocities, such a curve approximates the trajectory that a particle starting at the point of observation would have followed during the period of observation. Numbers indicate days of the month. Note the persistent veering to the right, at a period of about 14 h, which is the value of $2\pi/f$ at that latitude (57.8°N). (*From Gustafson & Kullenberg, 1936, as adapted by Gill, 1982*)

based on first-order forward differencing yields the simplest discretization of Eqs. (2.11):

$$\frac{\mathrm{d}u}{\mathrm{d}t} - fv = 0 \longrightarrow \frac{\tilde{u}^{n+1} - \tilde{u}^n}{\Delta t} - f\tilde{v}^n = 0$$
$$\frac{\mathrm{d}v}{\mathrm{d}t} + fu = 0 \longrightarrow \frac{\tilde{v}^{n+1} - \tilde{v}^n}{\Delta t} + f\tilde{u}^n = 0.$$

The latter pair can be cast into a recursive form as follows:

$$\tilde{u}^{n+1} = \tilde{u}^n + f\Delta t\,\tilde{v}^n \tag{2.24a}$$
$$\tilde{v}^{n+1} = \tilde{v}^n - f\Delta t\,\tilde{u}^n. \tag{2.24b}$$

Thus, given initial values $\tilde{u}^0$ and $\tilde{v}^0$ at t^0, the solution can be computed easily at time t^1

$$\tilde{u}^1 = \tilde{u}^0 + f\Delta t\,\tilde{v}^0 \tag{2.25}$$
$$\tilde{v}^1 = \tilde{v}^0 - f\Delta t\,\tilde{u}^0. \tag{2.26}$$

Then, by means of the same algorithm, the solution can be obtained iteratively at times t^2, t^3, and so on (do not confuse the temporal index with an exponent here and in the following). Clearly, the main advantage of the preceding scheme is its simplicity, but it is not sufficient to render it acceptable, as we shall soon learn.

To explore the numerical error generated by the Euler method, we carry out Taylor expansions of the type

$$\tilde{u}^{n+1} = \tilde{u}^n + \Delta t\left[\frac{\mathrm{d}\tilde{u}}{\mathrm{d}t}\right]_{t=t^n} + \frac{\Delta t^2}{2}\left[\frac{\mathrm{d}^2\tilde{u}}{\mathrm{d}t^2}\right]_{t=t^n} + \mathcal{O}\left(\Delta t^3\right)$$

and similarly for $\tilde{v}$ to obtain the following expressions from Eqs. (2.24)

$$\left[\frac{\mathrm{d}\tilde{u}}{\mathrm{d}t} - f\tilde{v}\right]_{t=t^n} = -\left[\frac{\mathrm{d}^2\tilde{u}}{\mathrm{d}t^2}\right]_{t=t^n}\frac{\Delta t}{2} + \mathcal{O}\left(\Delta t^2\right) \tag{2.27a}$$
$$\left[\frac{\mathrm{d}\tilde{v}}{\mathrm{d}t} + f\tilde{u}\right]_{t=t^n} = -\left[\frac{\mathrm{d}^2\tilde{v}}{\mathrm{d}t^2}\right]_{t=t^n}\frac{\Delta t}{2} + \mathcal{O}\left(\Delta t^2\right). \tag{2.27b}$$

Differentiation of Eq. (2.27a) with respect to time and use of Eq. (2.27b) to eliminate $\mathrm{d}\tilde{v}/\mathrm{d}t$ allow us to recast Eq. (2.27a) into a simpler form, and similarly for Eq. (2.27b):

$$\frac{\mathrm{d}\tilde{u}^n}{\mathrm{d}t} - f\tilde{v}^n = \frac{f^2\Delta t}{2}\tilde{u}^n + \mathcal{O}\left(\Delta t^2\right) \tag{2.28a}$$
$$\frac{\mathrm{d}\tilde{v}^n}{\mathrm{d}t} + f\tilde{u}^n = \frac{f^2\Delta t}{2}\tilde{v}^n + \mathcal{O}\left(\Delta t^2\right). \tag{2.28b}$$

Obviously, the numerical scheme mirrors the original equations, except that an additional term appears in each right-hand side. This additional term takes the form of antifriction (friction would have a minus sign instead) and will therefore increase the discrete velocity over time.

The *truncation error* of the Euler scheme—the right-hand side of the preceding expressions—tends to zero as Δt vanishes, which is why the scheme is said to be *consistent*. The truncation is on the order of Δt at the first power, and the scheme is therefore said to be *first-order accurate*, which is the lowest possible level of accuracy. Nonetheless, this is not the chief weakness of the present scheme, since we must expect that the introduction of antifriction will create an unphysical acceleratation. Indeed, elementary manipulations

of the time-stepping algorithm (2.24) lead to $(\tilde{u}^{n+1})^2+(\tilde{v}^{n+1})^2 = (1+f^2\Delta t^2)\left\{(\tilde{u}^n)^2+(\tilde{v}^n)^2\right\}$ so that by recursion

$$||\tilde{\mathbf{u}}||^2=(\tilde{u}^n)^2+(\tilde{v}^n)^2=(1+f^2\Delta t^2)^n\left\{(\tilde{u}^0)^2+(\tilde{v}^0)^2\right\}. \tag{2.29}$$

Thus, although the kinetic energy (directly proportional to the squared norm $||\tilde{\mathbf{u}}||^2$) of the inertial oscillation must remain constant, as was seen in Section 2.3, the kinetic energy of the discrete solution increases without bound[2] even if the time step Δt is taken much smaller than the characteristic time $1/f$. Algorithm (2.24) is *unstable*. Because such a behavior is not acceptable, we need to formulate an alternative type of discretization.

In our first scheme, the time derivative was taken by going forward from time level t^n to t^{n+1} and the other terms at t^n, and the scheme became a recursive algorithm to calculate the next values from the current values. Such a discretization is called an *explicit scheme*. By contrast, in an *implicit scheme*, the terms other than the time derivatives are taken at the new time t^{n+1} (which is similar to taking a backward difference for the time derivative):

$$\frac{\tilde{u}^{n+1}-\tilde{u}^n}{\Delta t}-f\tilde{v}^{n+1}=0 \tag{2.30a}$$

$$\frac{\tilde{v}^{n+1}-\tilde{v}^n}{\Delta t}+f\tilde{u}^{n+1}=0. \tag{2.30b}$$

In this case, the norm of the discrete solution decreases monotonically toward zero, according to

$$(\tilde{u}^n)^2+(\tilde{v}^n)^2=(1+f^2\Delta t^2)^{-n}\left\{(\tilde{u}^0)^2+(\tilde{v}^0)^2\right\}. \tag{2.31}$$

This scheme can be regarded as *stable*, but as the kinetic energy should neither decrease or increase, it may rather be considered as *overly stable*.

Of interest is the family of algorithms based on a weighted average between explicit and implicit schemes:

$$\frac{\tilde{u}^{n+1}-\tilde{u}^n}{\Delta t}-f\left[(1-\alpha)v^n+\alpha\tilde{v}^{n+1}\right]=0 \tag{2.32a}$$

$$\frac{\tilde{v}^{n+1}-\tilde{v}^n}{\Delta t}+f\left[(1-\alpha)u^n+\alpha\tilde{u}^{n+1}\right]=0, \tag{2.32b}$$

with $0 \leq \alpha \leq 1$. The numerical scheme is explicit when $\alpha=0$ and implicit when $\alpha=1$. Hence, the coefficient α may be regarded as the degree of implicitness in the scheme. It has a crucial impact on the time evolution of the

[2]From the context, it should be clear that ^{n} in $(1+f^2\Delta t^2)^n$ is an exponent, whereas in $\tilde{u}^n$, it is the time index. In the following text, we will not point out this distinction again, leaving it to the reader to verify the context.

kinetic energy:

$$(\tilde{u}^n)^2+(\tilde{v}^n)^2=\left[\frac{1+(1-\alpha)^2f^2\Delta t^2}{1+\alpha^2f^2\Delta t^2}\right]^n\left\{(\tilde{u}^0)^2+(\tilde{v}^0)^2\right\}. \tag{2.33}$$

According to whether α is less than, equal to, or greater than $1/2$, the kinetic energy increases, remains constant, or decreases over time. It seems therefore appropriate to select the scheme with $\alpha=1/2$, which is usually said to be *semi-implicit*.

It is now instructive to compare the semi-implicit approximate solution with the exact solution (2.12). For this to be relevant, the same initial conditions are prescribed, that is, $\tilde{u}^0=V\sin\phi$ and $\tilde{v}^0=V\cos\phi$. Then, at any time t^n, the discrete velocity may be shown (see Numerical Exercise 2.9) to be

$$\tilde{u}^n=V\sin(\tilde{f}t^n+\phi)$$
$$\tilde{v}^n=V\cos(\tilde{f}t^n+\phi),$$

with the angular frequency $\tilde{f}$ given by

$$\tilde{f}=\frac{1}{\Delta t}\arctan\left(\frac{f\Delta t}{1-f^2\Delta t^2/4}\right). \tag{2.34}$$

Although the amplitude of the oscillation (V) is correct, the numerical angular frequency, $\tilde{f}$, differs from the true value f. However, the smaller the dimensionless product $f\Delta t$, the smaller the error:

$$\tilde{f}\to f\left(1-\frac{f^2\Delta t^2}{12}\right)\quad\text{as}\quad f\Delta t\to 0.$$

In other words, selecting a time increment Δt much shorter than $1/f$, the time scale of inertial oscillations, leads to a frequency that is close to the exact one.

2.7 NUMERICAL CONVERGENCE AND STABILITY

A Taylor-series expansion performed on the discrete equations of the inertial oscillations revealed that the truncation error vanishes as Δt tends to zero. However, we are not so much interested in verifying that the limit of the discretized equation for increasing resolution returns the exact equation (*consistency*) as we are in making sure that the *solution* of the discretized equation tends to the *solution* of the differential equations (i.e., the exact solution). If the difference between the exact and discrete solutions tends to zero as Δt vanishes, then the discretization is said to *converge*.

Unfortunately proving convergence is not a trivial task, especially as we generally do not know the exact solution, in which case the use of numerical discretization would be superfluous. Furthermore, the exact solution of the discrete equation can very rarely be written in a closed form because the discretization only provides a method, an *algorithm*, to construct the solution in time.

Without knowing precisely the solutions of either the continuous problem or its discrete version, direct proofs of convergence involve mathematics well beyond the scope of the present book and will be not pursued here. We will, however, rely on a famous theorem called the *Lax–Richtmyer equivalence theorem* (Lax & Richtmyer, 1956), which states that

A consistent finite-difference scheme for a linear partial differential equation for which the initial value problem is well posed is convergent if and only if it is stable.

So, while proof of convergence is a mathematical exercise for researchers well versed in functional analysis, we will restrict ourselves here and in every other instance across the book to verify consistency and stability and will then invoke the theorem to claim convergence. This is a particularly interesting approach not only because checking stability and consistency is much easier than proving convergence but also because stability analysis provides further insight in propagation properties of the numerical scheme (see Section 5.4). There remains, however, to define stability and to design efficient methods to verify the stability of numerical schemes. Our analysis of the explicit Euler scheme (2.24) for the discretization of inertial oscillations led us to conclude that it is unstable because the velocity norm, and hence the energy of the system, gradually increases with every time step.

The adjective *unstable* seems quite natural in this context but lacks precision, and an exact definition is yet to be given. Imagine, for example, the use of an implicit Euler scheme (generally taken as the archetype of a stable scheme) on a standard linear differential equation:

$$\frac{\partial u}{\partial t} = \gamma u \quad \rightarrow \quad \frac{\tilde{u}^{n+1} - \tilde{u}^n}{\Delta t} = \gamma\, \tilde{u}^{n+1}. \tag{2.35}$$

We readily see that for $0 < \gamma \Delta t < 1$, the norm of $\tilde{u}$ increases:

$$\tilde{u}^n = \left(\frac{1}{1 - \gamma \Delta t} \right)^n \tilde{u}^0. \tag{2.36}$$

We would however hardly disqualify the scheme as unstable, since the numerical solution increases its norm simply because the exact solution $u = u^0 \mathrm{e}^{\gamma t}$ does so. In the present case, we can even show that the numerical solution actually converges to the exact solution:

$$\lim_{\Delta t \to 0} \tilde{u}^n = \tilde{u}^0 \lim_{\Delta t \to 0} \left(\frac{1}{1 - \gamma \Delta t} \right)^n = \tilde{u}^0 \lim_{\Delta t \to 0} \left(\frac{1}{1 - \gamma \Delta t} \right)^{t/\Delta t} = \tilde{u}^0 \mathrm{e}^{\gamma t}. \tag{2.37}$$

with $t = n \Delta t$.

Stability is thus a concept that should be related not only to the behavior of the discrete solution but also to the behavior of the exact solution. Loosely speaking, we will qualify a numerical scheme as unstable if its solution grows much faster than the exact solution and, likewise, overstable if its solution decreases much faster than the exact solution.

2.7.1 Formal Stability Definition

A mathematical definition of stability, one which allows the discrete solution to grow but only to a certain extent, is as follows. If the discrete state variable is represented by an array $\mathbf{x}$ (collecting into a single vector the values of all variables at all spatial grid points), which is stepped in time by an algorithm based on the selected discretization, the corresponding numerical scheme is said to be stable over a fixed time interval T if there exists a constant C such that

$$\|\mathbf{x}^n\| \leq C \|\mathbf{x}^0\| \tag{2.38}$$

for all $n\Delta t \leq T$. A scheme is thus stable if regardless of Δt ($\leq T$), the numerical solution remains bounded for $t \leq T$.

This definition of stability leaves the numerical solution quite some room for growth, very often well beyond what a modeler is willing to tolerate. This definition of stability is, however, the necessary and sufficient stability used in the Lax–Richtmyer equivalence theorem and is thus the one utilized to ascertain convergence. If we permit a slower rate of growth in the numerical solution, we will not destroy convergence. In particular, we could decide to use the so-called strict stability condition.

2.7.2 Strict Stability

For a system conserving one or several integral norms (such as total energy or wave action), we may naturally impose that the corresponding norm of the numerical solution does not grow at all over time:

$$\|\mathbf{x}^n\| \leq \|\mathbf{x}^0\| \,. \tag{2.39}$$

Obviously, a scheme that is stable in the sense of Eq. (2.39) is also stable in the sense of Eq. (2.38), whereas the inverse is not necessarily true. The more stringent definition (2.39) will be called *strict stability condition* and refers to the condition that the norm of the numerical solution is not allowed to increase at all.

2.7.3 Choice of a Stability Criterion

The choice of stability criterion will depend largely on the mathematical and physical problem at hand. For a wave propagation problem, for example, strict stability will be the natural choice (assuming some norm is conserved in the physical process), whereas for physically unbounded problems, the less stringent numerical stability definition (2.38) may be used.

We can now examine two previous discretization schemes in the light of these two stability definitions. For the explicit Euler discretization (2.24) of inertial oscillation, the scheme is unstable in the sense of Eq. (2.39) (and deserves this label in view of the required energy conservation), although it is technically

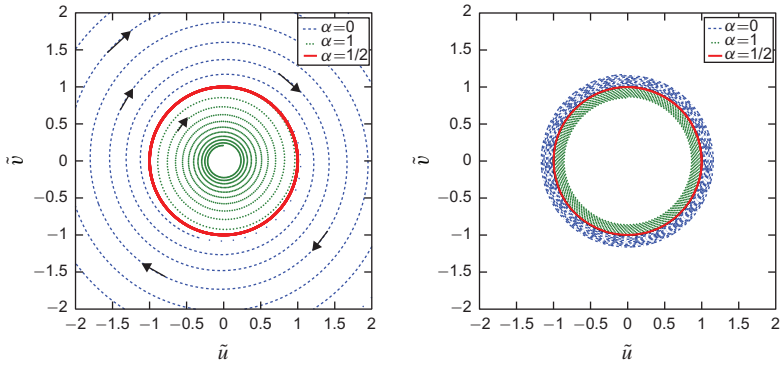

FIGURE 2.11 Representation (called a hodograph) of the numerical solution $(\tilde{u}, \tilde{v})$ (2.32a)–(2.32b) of the explicit discretization of the inertial oscillation ($\alpha = 0$), the implicit version ($\alpha = 1$), and the semi-implicit scheme ($\alpha = 1/2$). The hodograph on the left was obtained with $f\Delta t = 0.05$ and the one on the right panel with $f\Delta t = 0.005$. The inertial oscillation (Fig. 2.4) is clearly visible, but the explicit scheme induces spiralling out and the implicit scheme spiralling in. When the time step is reduced (moving from left panel to right panel), the solution approaches the exact solution. In both cases, 10 inertial periods were simulated.

stable in the sense of Eq. (2.38), as we will proceed to show. Since the norm of the velocity is, according to Eq. (2.29),

$$\|\tilde{\mathbf{u}}^n\| = \left(1 + f^2\Delta t^2\right)^{n/2} \|\tilde{\mathbf{u}}^0\|, \tag{2.40}$$

we simply need to demonstrate[3] that the amplification is limited by a constant independent of n and Δt:

$$\left(1 + f^2\Delta t^2\right)^{n/2} \leq \left(1 + f^2\Delta t^2\right)^{T/(2\Delta t)} \leq \mathrm{e}^{\frac{f^2\Delta t T}{2}} \leq \mathrm{e}^{\frac{f^2T^2}{2}}. \tag{2.42}$$

The scheme is thus stable in the sense of Eq. (2.38) and even if growth of the norm can be quite important, according to the Lax–Richtmyer equivalence theorem, the solution will converge as the time step is reduced. This is indeed what is observed (Fig. 2.11) and can be proved explicitly (see Numerical Exercise 2.5). In practice, however, the time step is never allowed to be very small for obvious computer constraints. Also, the time window T over which simulations take place can be very large, and any increase of the velocity norm is unacceptable even if the solution is guaranteed to converge for smaller time steps. For

[3] For the demonstration, we use the inequality

$$(1+a)^b \leq \mathrm{e}^{ab} \text{ for } a, b \geq 0, \tag{2.41}$$

which can be easily be proved by observing that $(1+a)^b = \mathrm{e}^{b\ln(1+a)}$ and that $\ln(1+a) \leq a$ when $a \geq 0$.

this reason, the strict stability condition (2.39) is preferred, and the semi-implicit Euler discretization is chosen.

In the second example, that of the implicit Euler scheme applied to the growth equation, the scheme (2.35) is stable in the sense of Eq. (2.38) (since it converges) but allows growth in the numerical solution in accordance with the exact solution.

Recapitulating the different concepts encountered in the numerical discretization, we now have a recipe to construct a convergent method: Design a discretization for which consistency (an equation-related property) can be verified by straightforward Taylor-series expansion, then check stability of the numerical scheme (some practical methods will be provided later), and finally invoke the Lax–Richtmyer equivalence theorem to prove convergence (a solution-related property). But, as the equivalence theorem is strictly valid only for linear equations, surprises may arise in nonlinear systems. We also have to mention that establishing convergence by this indirect method demands that initial and boundary conditions, too, converge to those of the continuous differential system. Finally, convergence is assured only for well-posed initial value problems. This, however, is not a concern here, since all geophysical fluid models we consider are physically well posed.

2.8 PREDICTOR-CORRECTOR METHODS

Till now, we have illustrated numerical discretizations on the linear equations describing inertial oscillations. The methods can be easily generalized to equations with a nonlinear source term Q in the equation governing the variable u, as

$$\frac{\mathrm{d}u}{\mathrm{d}t} = Q(t, u). \tag{2.43}$$

For simplicity, we consider here a scalar variable u, but extension to a state vector $\mathbf{x}$, such as $\mathbf{x} = (u, v)$, is straightforward.

The previous methods can be recapitulated as follows:

- The explicit Euler method (*forward scheme*):

$$\tilde{u}^{n+1} = \tilde{u}^n + \Delta t\, Q^n \tag{2.44}$$

- The implicit Euler method (*backward scheme*):

$$\tilde{u}^{n+1} = \tilde{u}^n + \Delta t\, Q^{n+1} \tag{2.45}$$

- The semi-implicit Euler scheme (*trapezoidal scheme*):

$$\tilde{u}^{n+1} = \tilde{u}^n + \frac{\Delta t}{2}\left(Q^n + Q^{n+1}\right) \tag{2.46}$$

- A general two-points scheme (with $0 \leq \alpha \leq 1$):

$$\tilde{u}^{n+1} = \tilde{u}^n + \Delta t \left[(1-\alpha) Q^n + \alpha Q^{n+1} \right]. \tag{2.47}$$

Note that these schemes may be interpreted either as finite-difference approximations of the time derivative or as finite-difference approximations of the time integration of the source term. Indeed,

$$u(t^{n+1}) = u(t^n) + \int_{t^n}^{t^{n+1}} Q \, \mathrm{d}t, \tag{2.48}$$

and the various schemes can be viewed as different ways of approximating the integral, as depicted in Fig. 2.12. All discretization schemes based on the exclusive use of Q^n and Q^{n+1} to evaluate the integral between t^n and t^{n+1}, which are called *two-point methods*, are inevitably first-order methods, except the semi-implicit (or trapezoidal) scheme, which is of second order. Second order is thus the highest order achievable with a two-point method. To achieve an order higher than two, denser sampling of the Q term must be used to approximate the time integration.

Before considering this, however, a serious handicap should be noted: The source term Q depends on the unknown variable $\tilde{u}$, and we face the problem

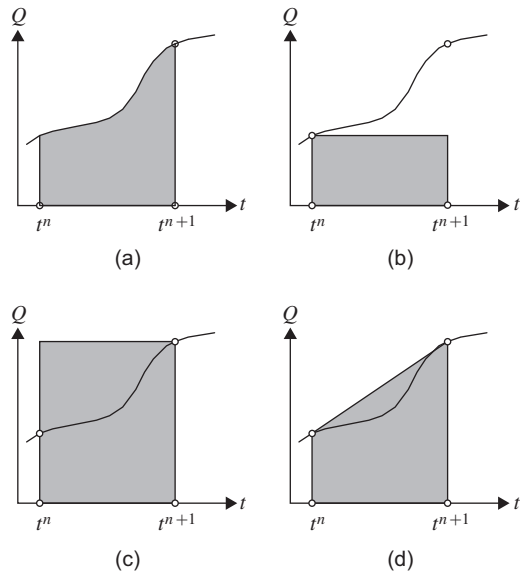

FIGURE 2.12 Time integration of the source term Q between t^n and t^{n+1}: (a) exact integration, (b) explicit scheme, (c) implicit scheme, and (d) semi-implicit, trapezoidal scheme.

of not being able to calculate Q^{n+1} *before* we know $\tilde{u}^{n+1}$, which is to be calculated from the value of Q^{n+1}. There is a vicious circle here! In the original case of inertial oscillations, the circular dependence was overcome by an algebraic manipulation of the equations prior to solution (gathering all $n+1$ terms on the left), but when the source term is nonlinear, as is often the case, such preliminary manipulation is generally not possible, and we need to circumvent the exact calculation by searching for a good approximation.

Such an approximation may proceed by using a first guess $\tilde{u}^\star$ in the Q term:

$$Q^{n+1} \simeq Q(t^{n+1}, \tilde{u}^\star), \tag{2.49}$$

as long as $\tilde{u}^\star$ is a sufficiently good estimate of $\tilde{u}^{n+1}$. The closer $\tilde{u}^\star$ is to $\tilde{u}^{n+1}$, the more faithful is the scheme to the ideal implicit value. If this estimate $\tilde{u}^\star$ is provided by a preliminary explicit (forward) step, according to:

$$\tilde{u}^\star = \tilde{u}^n + \Delta t\, Q(t^n, \tilde{u}^n) \tag{2.50a}$$

$$\tilde{u}^{n+1} = \tilde{u}^n + \frac{\Delta t}{2}\Big[Q(t^n, \tilde{u}^n) + Q(t^{n+1}, \tilde{u}^\star)\Big], \tag{2.50b}$$

we obtain a two-step algorithm, called the *Heun method*. It can be shown to be second-order accurate.

This second-order method is actually a particular member of a family of so-called *predictor-corrector methods*, in which a first guess $\tilde{u}^\star$ is used as a proxy for $\tilde{u}^{n+1}$ in the computation of complicated terms.

2.9 HIGHER-ORDER SCHEMES

If we want to go beyond second-order methods, we need to take into account a greater number of values of the Q term than those at t^n and t^{n+1}. We have two basic possibilities: either to include intermediate points between t^n and t^{n+1} or to use Q values at previous steps $n-1, n-2, \ldots$. The first approach leads to the so-called family of *Runge–Kutta methods* (or *multistage methods*), whereas the second generates the so-called *multistep methods*.

The simplest method, using a single intermediate point, is the so-called *midpoint method*. In this case (Fig. 2.13), the integration is achieved by first calculating the value $\tilde{u}^{n+1/2}$ (playing the role of $\tilde{u}^\star$) at an intermediate stage $t^{n+1/2}$ and then integrating for the whole step based on this midpoint estimate:

$$\tilde{u}^{n+1/2} = \tilde{u}^n + \frac{\Delta t}{2} Q\left(t^n, \tilde{u}^n\right) \tag{2.51a}$$

$$\tilde{u}^{n+1} = \tilde{u}^n + \Delta t\, Q\left(t^{n+1/2}, \tilde{u}^{n+1/2}\right). \tag{2.51b}$$

This method, however, is only second-order accurate and offers no improvement over the earlier Heun method (2.50).

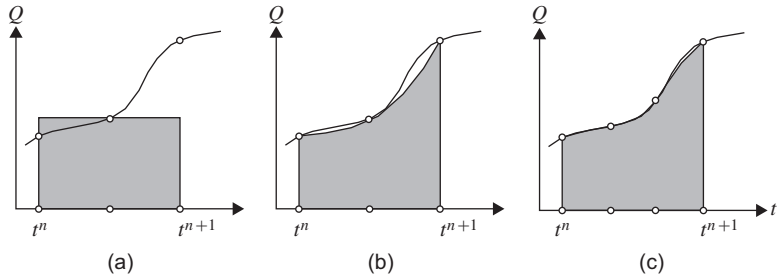

FIGURE 2.13 Runge–Kutta schemes of increasing complexity: (a) midpoint integration, (b) integration with parabolic interpolation, and (c) with cubic interpolation.

A popular fourth-order method can be constructed by using a parabolic interpolation between the values of Q with two successive estimates at the central point before proceeding with the full step:

$$\tilde{u}_a^{n+1/2} = \tilde{u}^n + \frac{\Delta t}{2} Q\left(t^n, \tilde{u}^n\right) \tag{2.52a}$$

$$\tilde{u}_b^{n+1/2} = \tilde{u}^n + \frac{\Delta t}{2} Q\left(t^{n+1/2}, \tilde{u}_a^{n+1/2}\right) \tag{2.52b}$$

$$\tilde{u}^\star = \tilde{u}^n + \Delta t\, Q\left(t^{n+1/2}, \tilde{u}_b^{n+1/2}\right) \tag{2.52c}$$

$$\begin{aligned}\tilde{u}^{n+1} = \tilde{u}^n + \Delta t \Bigg(& \frac{1}{6} Q\left(t^n, \tilde{u}^n\right) + \frac{2}{6} Q\left(t^{n+1/2}, \tilde{u}_a^{n+1/2}\right) \\ & + \frac{2}{6} Q\left(t^{n+1/2}, \tilde{u}_b^{n+1/2}\right) + \frac{1}{6} Q\left(t^{n+1}, \tilde{u}^\star\right)\Bigg).\end{aligned} \tag{2.52d}$$

We can increase the order by using higher polynomial interpolations (Fig. 2.13).

As mentioned earlier, instead of using intermediate points to increase the order of accuracy, we can exploit already available evaluations of Q from previous steps (Fig. 2.14). The most popular method in GFD models is the *leapfrog method*, which simply reuses the value at time step $n-1$ to "jump over" the Q term at t^n in a $2\Delta t$ step:

$$\tilde{u}^{n+1} = \tilde{u}^{n-1} + 2\Delta t\, Q^n. \tag{2.53}$$

This algorithm offers second-order accuracy while being fully explicit. An alternative second-order method using the value at $n-1$ is the so-called *Adams–Bashforth method*:

$$\tilde{u}^{n+1} = \tilde{u}^n + \Delta t \frac{\left(3Q^n - Q^{n-1}\right)}{2}, \tag{2.54}$$

which can be interpreted in the light of Fig. 2.14.

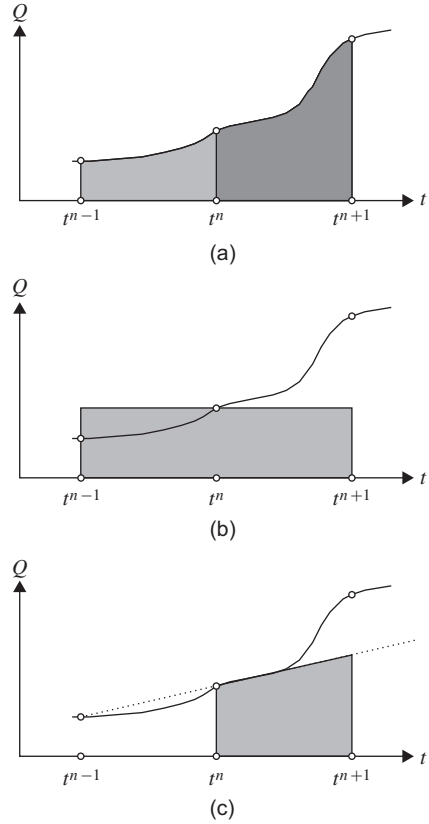

FIGURE 2.14 (a) Exact integration from t^{n-1} or t^n toward t^{n+1}, (b) leapfrog integration starts from t^{n-1} to reach t^{n+1}, whereas (c) Adams–Bashforth integration starts from t^n to reach t^{n+1}, using previous values to extrapolate Q over the integration interval t^n, t^{n+1}.

Higher-order methods can be constructed by recalling more points from the past $(n-2, n-3, ...)$, but we will not pursue this approach further for the following two reasons. First, using anterior points creates a problem at the start of the calculation from the initial condition. The first step must be different in order to avoid using one or several points that do not exist, and an explicit Euler scheme is usually performed. One such step is sufficient to initiate the leapfrog and Adams–Bashforth schemes, but methods that use earlier values (at $n-2, n-3, \ldots$) require more cumbersome care, which can amount to considerable effort in a GFD code. Second, the use of several points in the past demands a proportional increase in computer storage because values cannot be discarded as quickly before making room for newer values. Again, for a single equation, this is not much of a trouble, but in actual applications, size matters and only a few past values can be stored in the central memory of the machine. A similar

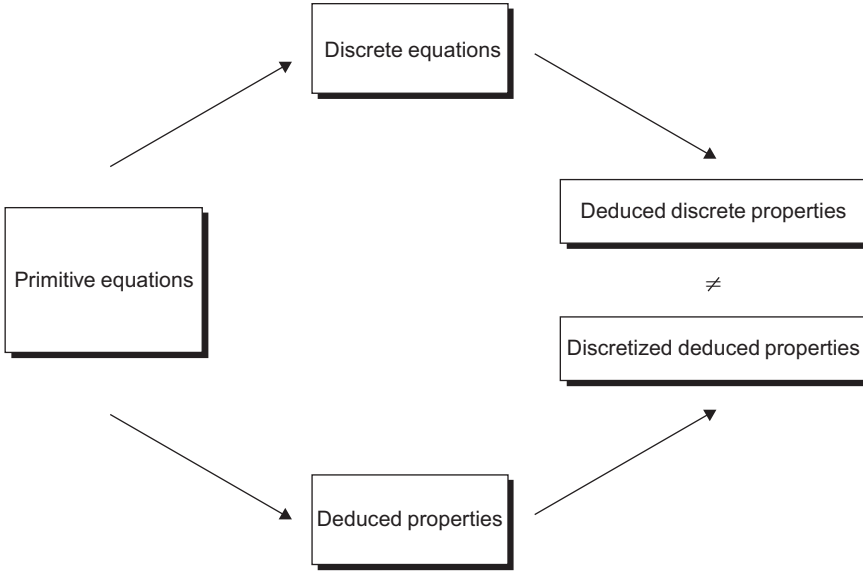

FIGURE 2.15 Schematic representation of discretization properties and mathematical properties interplay.

problem arises also with multistage methods, although these do not need any particular starting mechanism.

We can conclude the section by remarking that higher-order methods can always be designed but at the price of more frequent evaluations of the right-hand side of the equation (potentially a very complicated term) and/or greater storage of numerical values at different time steps. Since higher-order methods create more burden on the computation, we ought to ask whether they at least provide better numerical solutions than lower-order methods. We have therefore to address the question of accuracy of these methods, which will be considered in Section 4.8.

A fundamental difference between analytical solutions and numerical approximations emerges. For some equations, properties of the solution can be derived without actually solving the equations. It is easy to prove, for example, that the velocity magnitude remains constant during an inertial oscillation. The numerical solution on the other hand is generally not guaranteed to satisfy the same property as its analytical counterpart (the explicit Euler discretization did not conserve the velocity norm). Therefore, we cannot be sure that mathematical properties of the analytical solutions will also be present in the numerical solution. This might appear as a strong drawback of numerical methods but can actually be used to assess the quality of numerical schemes. Also, for numerical schemes with adjustable parameters (as the implicit factor), those parameters

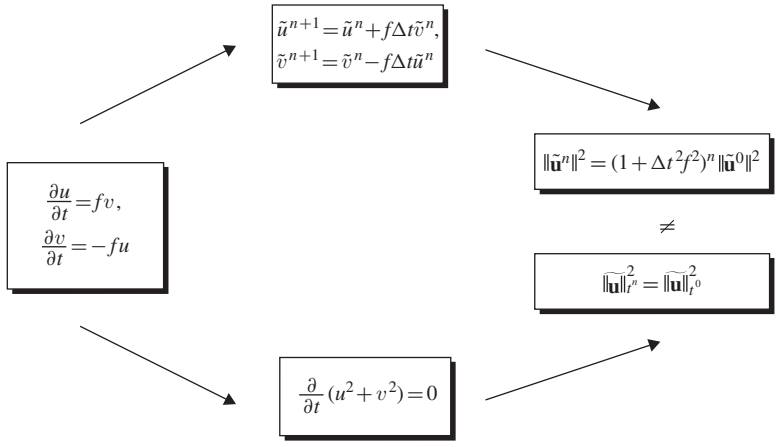

FIGURE 2.16 Schematic representation of discretization properties and mathematical properties interplay exemplified in the case of inertial oscillation.

can be chosen so that the numerical solution respects as best as possible the exact properties.

We can summarize by recognizing the fact that numerical solutions generally do not inherit the mathematical properties of the exact solution (Fig. 2.15), a handicap particularly easy to understand in the case of inertial oscillation and its discretization by an explicit scheme (Fig. 2.16). Later, we will encounter other properties (energy conservation, potential vorticity conservation, positiveness of concentrations, etc.) that can be used to guide the choice of parameter values in numerical schemes.

ANALYTICAL PROBLEMS

2.1. On Jupiter, a day lasts 9.9 Earth hours and the equatorial circumference is 448,600 km. Knowing that the measured gravitational acceleration at the equator is 26.4 m/s^2, deduce the true gravitational acceleration and the centrifugal acceleration.

2.2. The Japanese Shinkansen train (bullet train) zips from Tokyo to Ozaka (both at approximately 35°N) at a speed of 185 km/h. In the design of the train and tracks, do you think that engineers had to worry about the Earth's rotation? (*Hint*: The Coriolis effect induces an oblique force, the lateral component of which could produce a tendency of the train to lean sideways.)

2.3. Determine the lateral deflection of a cannonball that is shot in London (51°31′N) and flies for 25 s at an average horizontal speed of 120 m/s.

What would be the lateral deflection in Murmansk (68°52′N) and Nairobi (1°18′S)?

2.4. On a perfectly smooth and frictionless hockey field at Dartmouth College (43°38′N), how slowly should a puck be driven to perform an inertial circle of diameter equal to the field width (26 m)?

2.5. A stone is dropped from a 300-m high bridge at 35°N. In which cardinal direction is it deflected under the effect of the earth's rotation? How far from the vertical does the stone land? (Neglect air drag.)

2.6. At 43°N, raindrops fall from a cloud 2500 m above ground through a perfectly still atmosphere (no wind). In falling, each raindrop experiences gravity, a linear drag force with coefficient $C = 1.3\ \mathrm{s}^{-1}$ (i.e., the drag force in the x, y, and z directions is, respectively, $-Cu$, $-Cv$, and $-Cw$ per unit mass) and is also subjected to the three-dimensional Coriolis force. What is the trajectory of one raindrop? How far eastward and northward has the Coriolis force deflected the raindrop by the time it hits the ground? (*Hint*: It can be shown that the terminal velocity is reached very quickly relatively to the total falling time.)

2.7. A set of two identical solid particles of mass M attached to each other by a weightless rigid rod of length L are moving on a horizontal rotating plane in the absence of external forces (Fig. 2.17). As in geophysical fluid dynamics, ignore the centrifugal force caused by the ambient rotation. Establish the equations governing the motion of the set of particles, derive the most general solution, and discuss its physical implications.

2.8. At $t = 0$, two particles of equal mass M but opposite electrical charges q are released from rest at a distance L from each other on a rotating plane (constant rotation rate $\Omega = f/2$). Assuming as in GFD that the centrifugal force

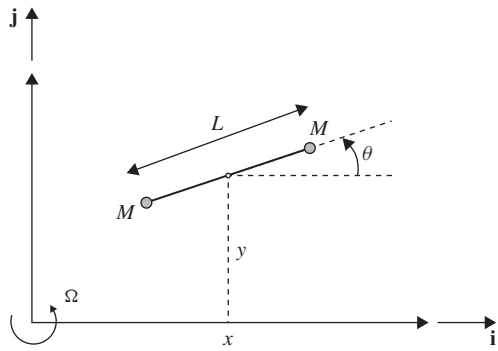

FIGURE 2.17 Two linked masses on a rotating plane (Problem 2.7).

caused by the ambient rotation is externally balanced, write the equations of motion of the two particles and the accompanying initial conditions. Then, show that the center of mass (the midpoint between the particles) is not moving, and write a differential equation governing the evolution of the distance $r(t)$ between the two particles. Is it possible that, as on a nonrotating plane, the electrical attraction between the two particles will make them collide ($r = 0$)?

2.9. Study the trajectory of a free particle of mass M released from a state of rest on a rotating, sloping, rigid plane (Fig. 2.18). The angular rotation rate is Ω, and the angle formed by the plane with the horizontal is α. Friction and the centrifugal force are negligible. What is the maximum speed acquired by the particle, and what is its maximum downhill displacement?

2.10. The curve reproduced in Fig. 2.19 is a progressive vector diagram constructed from current-meter observations at latitude 43°09′N in the Mediterranean Sea. Under the assumption of a uniform but time-dependent

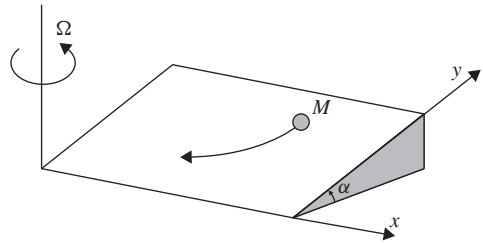

FIGURE 2.18 A free particle on a rotating, frictionless slope (Problem 2.9).

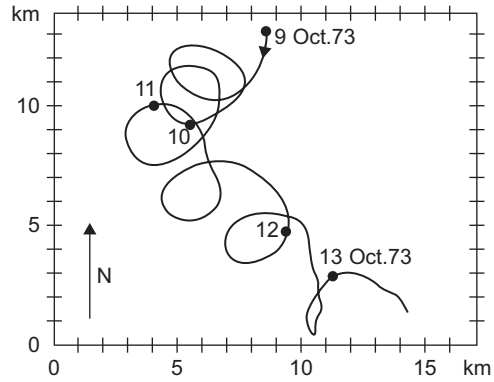

FIGURE 2.19 Progressive vector diagram constructed from current-meter observation in the Mediterranean Sea taken in October 1973 (Problem 2.10). (*Courtesy of Martin Mork, University of Bergen, Norway*)

flow field in the vicinity of the mooring, the curve can be interpreted as the trajectory of a water parcel. Using the marks counting the days along the curve, show that this set of observations reveals the presence of inertial oscillations. What is the average orbital velocity in these oscillations?

NUMERICAL EXERCISES

2.1. When using the semi-implicit scheme (2.32a)–(2.32b) with $\alpha = 1/2$, how many time steps are required per complete cycle (period of $2\pi/f$) to guarantee a relative error on f not exceeding 1%?

2.2. Develop an Euler scheme to calculate the position coordinates x and y of a particle undergoing inertial oscillations from its velocity components u and v, themselves calculated with an Euler scheme. Graph the trajectory $[\tilde{x}^n,\ \tilde{y}^n]$ for $n = 1, 2, 3, \ldots$ of the particle. What do you notice?

2.3. For the semi-implicit discretization of the inertial oscillation, calculate the number of complete cycles it takes before the exact solution and its numerical approximation are in phase opposition (180° phase shift). Express this number of cycles as a function of the parameter $f\Delta t$. What can you conclude for a scheme for which $f\Delta t = 0.1$ in terms of time windows that can be analyzed before the solution is out of phase?

2.4. Devise a leapfrog scheme for inertial oscillations and analyze its stability and angular frequency properties by searching for a numerical solution of the following form[4]:

$$\tilde{u}^n = V\varrho^n \sin(\tilde{f} n\Delta t + \phi), \quad \tilde{v}^n = V\varrho^n \cos(\tilde{f} n\Delta t + \phi).$$

2.5. Calculate the discrete solution of the explicit Euler scheme applied to inertial oscillations by searching for a solution of the same form as in Problem 2.4 where ϱ and $\tilde{f}$ are again parameters to be determined. Show that the discrete solution converges to the exact solution (2.12).

2.6. Prove the assertion that scheme (2.51) is of second order.

2.7. Adapt `coriolisdis.m` for a discretization of inertial oscillation with a frictional term

$$\frac{\mathrm{d}u}{\mathrm{d}t} = fv - cu \tag{2.55}$$

$$\frac{\mathrm{d}v}{\mathrm{d}t} = -fu - cv, \tag{2.56}$$

where $c = f\ k$. Run the explicit discretization with increasing values of k in $[0, 1]$. For which value of k does the explicit Euler discretization give

[4]For ϱ^n, n is an exponent, not an index.

you a solution with constant norm? Can you interpret this result in view of Eq. (2.28)?

2.8. Try several time discretization methods on the following set of equations:

$$\frac{\mathrm{d}u}{\mathrm{d}t} = fv \tag{2.57}$$

$$\frac{\mathrm{d}v}{\mathrm{d}t} = -fu + fk(1-u^2)v, \tag{2.58}$$

with initial condition $u=2$, $v=0$ at $t=0$. Use two values for the parameter k: first, $k=0.1$ and then $k=1$. Finally, try $k=5$. What do you notice?

2.9. Prove that an inertial oscillation with modified angular frequency (2.34) is the exact solution of the semi-implicit scheme (2.32). (*Hint*: Insert the solution into the finite-difference equations and find a condition on $\tilde{f}$.)

Pierre Simon Marquis de Laplace
1749–1827

From humble roots in rural France, Pierre Simon Laplace distinguished himself early by his abilities and went on to Paris. There, at the Académie des Sciences, Jean D'Alembert recognized the talents of the young Laplace and secured for him a position in the military school. Set with this appointment, Laplace began a study of planetary motions, which led him to make advances in integral calculus and differential equations. Skillful at changing his political views during the turbulent years of the French Revolution, Laplace managed to survive and continued his research almost without interruption. In 1799, he published the first volume of a substantial memoir titled *Mécanique Céleste*, which later grew into a five-volume treatise and has since been regarded as a cornerstone of classical physics. Some have said that this work is Isaac Newton's *Principia* (of 1687) translated in the language of differential calculus with the clarification of many important points that had remained puzzling to Newton. One such aspect is the theory of ocean tides, which Laplace was the first to establish on firm mathematical grounds.

The name Laplace is attached today to a differential operator (the sum of second derivatives), which arises in countless problems of physics, including geophysical fluid dynamics (see Chapter 16). (*Portrait taken from a nineteenth century colored engraving, The Granger Collection, New York*)

Gaspard Gustave de Coriolis
1792–1843

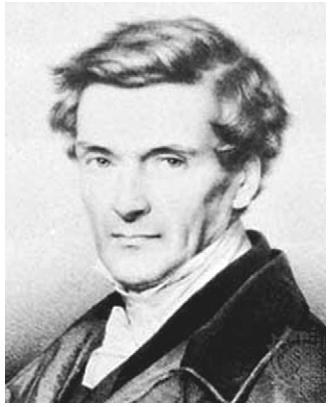

Born in France and trained as an engineer, Gaspard Gustave de Coriolis began a career in teaching and research at age 24. Fascinated by problems related to rotating machinery, he was led to derive the equations of motion in a rotating framework of reference. The result of these studies was presented to the Académie des Sciences in the summer of 1831. In 1838, Coriolis stopped teaching to become director of studies at the Ecole Polytechnique, but his health declined quickly and he died a few short years later.

The world's largest experimental rotating table, at the Institut de Mécanique in Grenoble, France, is named after him and has been used in countless simulations of geophysical fluid phenomena. (*Photo from the archives of the Académie des Sciences, Paris*)